A triad of residues is functionally transferrable between 5-HT$_3$ serotonin receptors and nicotinic acetylcholine receptors

Received for publication, August 3, 2017, and in revised form, November 29, 2017 Published, Papers in Press, January 3, 2018, DOI 10.1074/jbc.M117.810432

Richard Mosesso and Dennis A. Dougherty[1]

From the Division of Chemistry and Chemical Engineering, California Institute of Technology, Pasadena, California 91125

Edited by F. Anne Stephenson

Cys-loop receptors are pentameric ligand-gated ion channels that facilitate communication within the nervous system. Upon neurotransmitter binding, these receptors undergo an allosteric activation mechanism connecting the binding event to the membrane-spanning channel pore, which expands to conduct ions. Some of the earliest steps in this activation mechanism are carried out by residues proximal to the binding site, the relative positioning of which may reflect functional differences among members of the Cys-loop family of receptors. Herein, we investigated key side-chain interactions near the binding site via mutagenesis and two-electrode voltage-clamp electrophysiology in serotonin-gated 5-HT$_{3A}$ receptors (5-HT$_{3A}$Rs) and nicotinic acetylcholine receptors (nAChRs) expressed in *Xenopus laevis* oocytes. We found that a triad of residues aligning to Thr-152, Glu-209, and Lys-211 in the 5-HT$_{3A}$R can be exchanged between the homomeric 5-HT$_{3A}$R and the muscle-type nAChR α-subunit with small functional consequences. Via triple mutant cycle analysis, we demonstrated that this triad forms an interdependent network in the muscle-type nAChR. Furthermore, nAChR-type mutations of the 5-HT$_{3A}$R affect the affinity of nicotine, a competitive antagonist of 5-HT$_{3A}$Rs, in a cooperative manner. Using mutant cycle analyses between the 5-HT$_{3A}$ triad, loop A residues Asn-101 and Glu-102, β9 residue Lys-197, and the channel gate at Thr-257, we observed that residues in this region are energetically linked to the channel gate and are particularly sensitive to mutations that introduce a net positive charge. This study expands our understanding of the differences and similarities in the activation mechanisms of Cys-loop receptors.

Cys-loop receptors are the subset of pentameric ligand-gated ion channels found in vertebrates, and include excitatory nicotinic acetylcholine receptors (nAChRs)[2] and serotonin-activated 5-HT$_3$ receptors (5-HT$_3$Rs), as well as inhibitory type A γ-aminobutyric acid receptors (GABA$_A$Rs), and glycine receptors (GlyRs) (1–4). The pharmacology of these receptors is quite broad, and targeted therapeutics may lead to novel treatments for a variety of conditions (5–7).

The overall structure of Cys-loop receptors is highly conserved (8). Each subunit is composed of an extracellular domain (ECD) β sandwich, a transmembrane domain formed by four α-helices (numbered M1-M4), and a variable intracellular domain defined primarily by the loop between the M3 and M4 helices. Five subunits assemble in a concentric manner to form a single receptor. Ligand-binding sites are formed at subunit interfaces in the ECD by three primary (+) face "loops" A–C, and three complementary (−) face loops D–F. An overall picture of the interface between two subunits, as exemplified in the crystal structure of the homopentameric 5-HT$_{3A}$ receptor, is shown in Fig. 1*A* (PDB code 4PIR) (9).

The advent of complete structures of eukaryotic Cys-loop receptors, whereas generally at fairly low resolution, has provided valuable guidance for comparing members of the Cys-loop receptor family. The present work was motivated by the recognition of a triad of residues that are, in a global sense, conserved across several members of the family. Our primary focus has been on the homopentameric 5-HT$_{3A}$R, for which the residues of interest are Thr-152, Glu-209, and Lys-211 (Fig. 1*A*; numbering as in the crystal structure; these have been referred to elsewhere at Thr-179, Glu-236, and Lys-238). The structurally aligning residues in the α-subunits of the recently reported heteromeric $\alpha4\beta2$ nAChR (PDB code 5KXI) (10) are Lys-145, Asp-200, and Thr-202, whereas those in the $\beta3$ GABA$_A$ homopentamer are Glu-153, Arg-207, and Ser-209 (PDB code 4COF) (11). In each triad, there is a cationic residue (Lys/Arg), an anionic residue (Asp/Glu), and a residue with an alcohol side chain (Ser/Thr). However, the relative positioning of these functionalities varies among these receptors, which led us to ask whether the arrangement reflects differences among receptors. To facilitate comparison, we have designated the three sites as A, B, and C (Fig. 1*A*). A sequence alignment (Fig. 1*B*) illustrates the conservation of these arrangements within individual receptor subfamilies in humans. Note that there are exceptions in the $\alpha5$ and $\alpha10$ nAChR subunits, however, these particular α-subunits do not contribute to the primary binding face of

This work was supported by National Institutes of Health Grant NS 34407 and Training Grant NIH/NRSA T32 GM07616. The authors declare that they have no conflicts of interest with the contents of this article. The content is solely the responsibility of the authors and does not necessarily represent the official views of the National Institutes of Health.

This article contains Tables S1–S3 and Figs. S1–S8.

[1] To whom correspondence should be addressed: Dept. of Chemistry and Chemical Engineering, California Institute of Technology, Crellin 359, 1200 E. California Blvd., Pasadena, CA 91125. Tel.: 626-395-6089; Fax: 626-564-9297; E-mail: dadoc@caltech.edu.

[2] The abbreviations used are: nAChR, nicotinic acetylcholine receptor; 5-HT$_{3A}$R, serotonin type-3A receptor; GABA$_A$Rs, γ-aminobutyric acid receptors; GlyRs, glycine receptors; ECD, extracellular domain; 5-HT, 5-hydroxytryptamine; AcH, acetylcholine; PDB, Protein Data Bank.

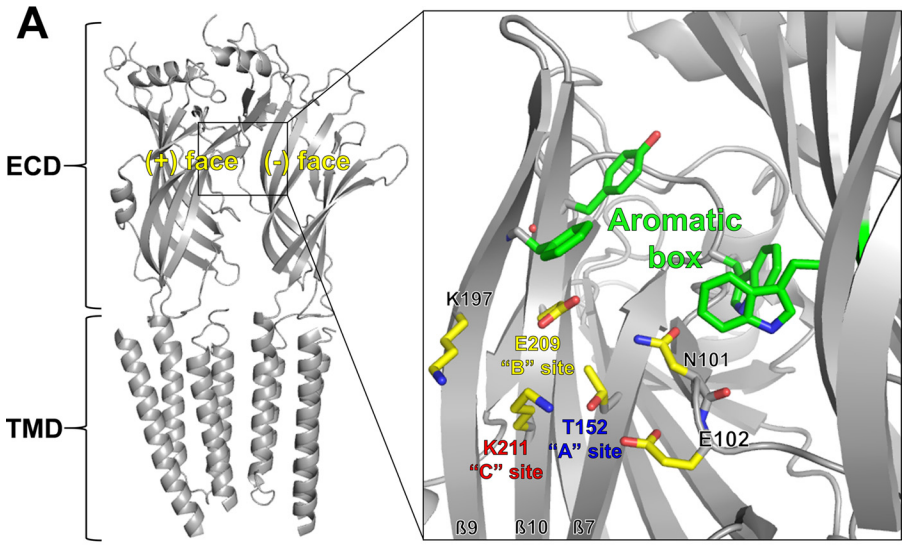

B

Residue number*:	...	152	...	209	210	211	...
human 5-HT$_{3A}$	...	T	...	E	M	K	...
human α1 nAChR	...	K	...	D	I	T	...
human α2 nAChR	...	K	...	D	V	T	...
human α3 nAChR	...	K	...	D	I	T	...
human α4 nAChR	...	K	...	D	I	T	...
human α5 nAChR	...	K	...	Y	I	T	...
human α6 nAChR	...	K	...	D	I	T	...
human α7 nAChR	...	K	...	D	V	T	...
human α9 nAChR	...	T	...	D	V	T	...
human α10 nAChR	...	T	...	D	V	T	...
human ß1 GABAA	...	E	...	R	L	S	...
human ß2 GABAA	...	E	...	R	L	S	...
human ß3 GABAA	...	E	...	R	L	S	...

Figure 1. Region of interest in this study. *A*, view of two adjacent receptor subunits from the 5-HT$_{3A}$R crystal structure (PDB code 4PIR). The *inset* shows residues mutated in this study highlighted in *yellow* and binding-site residues of the aromatic box shown in *green* for context; *red* = oxygen, *blue* = nitrogen. *B*, sequence alignment of subunits contributing to the primary binding face of human-type 5-HT$_{3A}$Rs, nAChRs, and GABA$_A$Rs. Cells are colored according to side-chain chemistry. *Unfilled cells* indicate non-conservation with regard to the triad in that receptor subtype. *TMD*, transmembrane domain; *ICD*, intracellular domain. *, Residue numbers corresponding to the 5-HT$_{3A}$R crystal structure (PDB code 4PIR). See "Experimental procedures" for sequence accession numbers.

nAChRs (1). The α8 nAChR subunit was excluded because it is not found in mammals (1).

Herein we evaluate the functional role of this triad in two excitatory Cys-loop receptors, the 5-HT$_{3A}$R and the muscle-type ($(\alpha_1)_2\beta_1\gamma\delta$) nAChR, using two-electrode voltage-clamp electrophysiology of mutant receptors expressed in *Xenopus laevis* oocytes. We find that the 5HT$_{3A}$R and nAChR triads can be swapped between these two receptors with minimal functional consequences. Additionally, substituting the nAChR triad into the 5-HT$_{3A}$R increases the affinity for nicotine, demonstrating that this triad influences ligand binding. In contrast, swapping the triad from the inhibitory GABA$_A$R into the 5HT$_{3A}$R does not result in a functional receptor.

We note from the start that several of the residues considered here have been evaluated by other investigators, and we have built off that work. In muscle-type nAChRs, state-dependent interactions have been proposed between Lys-145, Asp-200, and Tyr-190 (12–17). The former two residues are part of the above-described "triad," and Tyr-190 sits on loop C and is part of the aromatic box that contributes to the agonist-binding site (18, 19). The key hydrogen bonding role proposed for Tyr-190, however, is not possible in the 5-HT$_{3A}$R, as the aligning residue is Phe-199. As described below, a more general interaction between the triad of interest and loop A of the agonist-binding site is seen. Overall, these results highlight similarities and variations across members of the Cys-loop family.

Results

Effects of exchanging triads between 5-HT$_{3A}$ and the muscle-type nAChR

To evaluate the role of the triad of residues, we used site-directed mutagenesis to introduce mutations into receptors expressed in *X. laevis* oocytes and measured functional responses via dose-response relationships using two-electrode voltage-clamp electrophysiology, as described under "Experimental procedures." We generated the 5-HT$_{3A}$R single mutants T152K, E209D, and K211T, (corresponding to the nAChR residues at sites A, B, and C, respectively) as well at the double mutants AB, BC, and AC and the triple mutant ABC. The dose-response curves measured for all of these mutant receptors are compared in Fig. 2*A*, and the full pharmacological characterization in response to the native agonist serotonin (5-hydroxytryptamine, or 5-HT) is provided in Table 1. Representative two-electrode voltage-clamp traces are provided in Fig. S1. Relative to the wildtype 5-HT$_{3A}$R, the single mutant

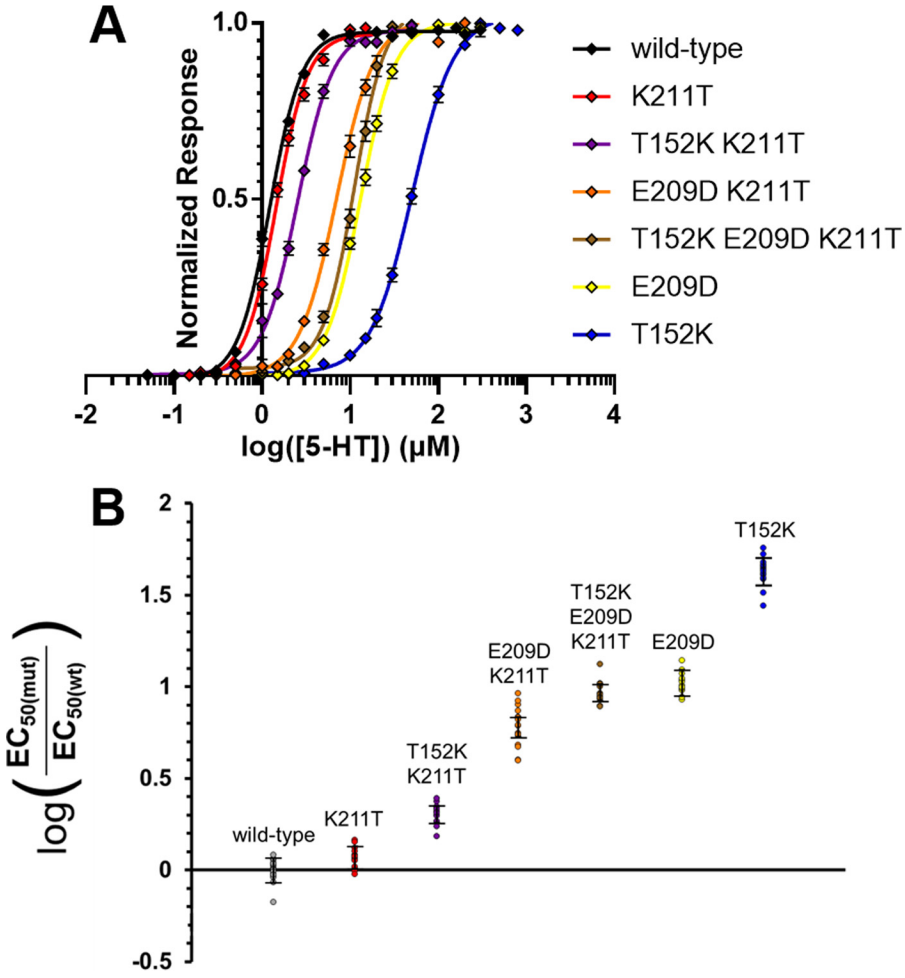

Figure 2. Mutating residues Thr-152, Glu-E209, and Lys-211 in 5-HT$_{3A}$Rs to their equivalents in nAChRs has non-additive effects on receptor function. *A*, dose-response curves (±S.E.) of wildtype and mutant receptors to 5-HT. Variants are ordered from top to bottom in order of increasing EC_{50}. *B*, scatterplots illustrating losses of function (±S.D.) of mutants on a logarithmic scale. The double mutants and triple mutant display considerable deviations from additivity.

Table 1
Response to 5-HT of 5-HT$_{3A}$Rs incorporating nAChR-type mutations

Mutation(s)	EC_{50} (μM)	n_H	$\lvert I_{max}\rvert$ (μA)	-Fold	*n*	$\Delta\Delta G^a$
Wildtype	1.3 ± 0.03	2.4 ± 0.11	1.1–78	1.0	21	
T152K	49 ± 1.03	1.9 ± 0.06	0.14–11	39	15	
E209D	13 ± 0.20	2.3 ± 0.07	0.53–21	10	15	
K211T	1.5 ± 0.04	2.9 ± 0.16	1.9–25	1.2	15	
T152K/E209D	NR[b]	NR	NR	NR	15	0.04[c]
T152K/K211T	2.5 ± 0.05	2.1 ± 0.08	1.3–56	2.0	14	1.8
E209D/K211T	6.9 ± 0.25	2.1 ± 0.11	0.18–12	5.5	16	0.49
T152K/E209D/K211T	11 ± 0.39	2.4 ± 0.18	0.15–19	8.4	12	

[a] kcal mol^{-1}.
[b] NR, no response.
[c] Measured in the background of K211T.

receptors had EC_{50} values for serotonin that were 39-, 10-, and 1.2-fold greater than wildtype for A, B, and C, respectively. Although the loss of function for receptors mutated at the A and B sites is clearly meaningful, the consequence of mutation at C is not. Note that structurally, however, the mutation at site B (Glu to Asp) would be expected to be the least perturbing.

Next, double mutants incorporating each of the above three mutations in pairs were generated to evaluate energetic coupling between the mutations via mutant cycle analyses. The extent of energetic coupling in a mutant cycle analysis is defined as the $\Delta\Delta G^0$ value for the double mutant, and quantifies the extent to which the individual mutations cooperate in the activation mechanism of the receptor (20). If residues are close enough in space that a direct interaction is possible, the $\Delta\Delta G^0$ value can also be used as a readout of the strength of this interaction.

The results of the double mutant cycles are provided in Table 1. Fig. 2*B* illustrates the non-additive effects of the mutations as a scatterplot. The AC double mutant had an EC_{50} of only 2.5 ± 0.05 μM 5-HT, a mere 2-fold loss of function relative to wildtype (1.3 ± 0.03 μM) and a 19-fold gain of function relative to the single mutant at A (EC_{50} = 49 ± 1.03 μM). Thus, these two mutations are strongly energetically coupled, with $\Delta\Delta G^0$ = 1.8 kcal mol^{-1}. This and their close orientation in space suggest a

direct interaction between these two residues. The double mutant BC showed a much lower coupling energy of $\Delta\Delta G^0 = 0.49$ kcal mol^{-1}. We consider a 2-fold deviation from additivity ($\Delta\Delta G^0 \geq 0.40$ kcal mol^{-1}) to be meaningful, suggesting that the B and C mutations do affect one another, albeit much less so than the AC double mutant. Fig. 2*B* compares the loss of function for each combination of mutations to wildtype.

The double mutant AB was nonfunctional up to 800 μM 5-HT. To meet our criterion for a meaningful coupling energy of $\geq$0.40 kcal mol^{-1}, the EC_{50} would either have to be less than 200 μM if the mutations are meaningfully subadditive or greater than 810 μM 5-HT if they are superadditive. The effects of the A and B mutations are clearly not subadditive, as we observed no response to concentrations of 5-HT up to 800 μM. It remains possible that the effects of these mutations are superadditive. If this were the case, we unfortunately could not measure a dose-response relationship due to open channel block of 5-HT_{3A}Rs at high concentrations of 5-HT. It is also possible that combining the A and B mutations impairs proper folding or trafficking of receptors to the cell surface.

Having generated the single mutants and double mutants, we next generated the triple mutant 5-HT_{3A}R T152K/E209D/K211T, "ABC," incorporating all three residues of the nicotinic triad. This receptor had only an 8.4-fold increase in 5-HT EC_{50} relative to wildtype. Thus, the full three-residue swap of nAChR residues into the 5-HT_{3A}R produces functional receptors. In fact, EC_{50} for the triple mutant is comparable with that for the single mutation at B and much less than the single mutation at A. The increase in EC_{50} for the triple mutant is much less than would be expected if the effects of the A, B, and C mutations were additive (Fig. 2*B*).

Having the triple mutant enables a double mutant cycle between the A and B sites in the background of the C mutation. This mutant cycle has a $\Delta\Delta G^0 = 0.04$ kcal mol^{-1} (Table 1), suggesting that A (T152K) and B (E209D) affect the receptor in distinct ways, at least in the background of K211T. The triple mutant also had somewhat different apparent activation/deactivation kinetics than wildtype receptors, and a greater extent of open channel block at concentrations of 5-HT above those that caused a maximal response (Fig. S2).

We next tested to see how a prototypical nAChR, the muscle-type ($(\alpha1)_2\beta1\gamma\delta$) nAChR, would respond when the 5-HT_{3A}R triad was introduced. Although the most recent nAChR structural data are for the $\alpha4\beta2$ neuronal subtype (10), we were unable to perform the desired experiments in that subtype due to poor expression levels. This has been addressed previously (21) by introducing the channel pore mutation L9′A, however, this would complicate our analysis, as the residues of interest are involved in receptor gating. However, the muscle-type nAChR expresses robustly in *Xenopus* oocytes. The relevant residues are the same in the $\alpha1$ (muscle-type) and $\alpha4$ subunits, and they are positioned similarly in the cryo-EM structure of the highly homologous *Torpedo* receptor (PDB code 2BG9) (22). We generated single mutants $\alpha1$ K145T, D200E, and T202K (A, B, and C), and the pharmacological responses of these mutants to the native agonist acetylcholine (ACh) are summarized in Table 2. Representative two-electrode voltage-clamp traces are provided in Fig. S3, and comparisons of the dose-response relationships between the mutant receptors and wildtype can be found in Fig. S4. All mutations caused modest losses of function: 4.9-, 2.9-, and 9.0-fold for A, B, and C, respectively.

Table 2
Response to ACh of muscle-type nAChRs incorporating 5-HT_{3A}R-type mutations

Mutation(s)	EC_{50} (μM)	n_H	$\lvert I_{max}\rvert$ (μA)	-Fold	n	$\Delta\Delta G^a$
Wildtype	15 ± 0.08	1.5 ± 0.08	3.6–47		14	
$\alpha1$ K145T	75 ± 3.6	1.4 ± 0.05	4.0–62	4.9	16	
$\alpha1$ D200E	45 ± 0.20	1.2 ± 0.08	0.05–0.58	2.9	13	
$\alpha1$ T202K	140 ± 2.5	1.5 ± 0.03	10–62	9.0	10	
$\alpha1$ K145T/D200E	44 ± 2.4	1.2 ± 0.09	0.08–23	2.8	13	0.94
$\alpha1$ K145T/T202K	110 ± 0.95	1.3 ± 0.04	0.35–5.9	7.2	12	1.0
$\alpha1$ D200E/T202K	82 ± 3.8	1.4 ± 0.08	0.05–0.14	5.3	10	0.93
$\alpha1$ K145T/D200E/T202K	67 ± 5.3	1.1 ± 0.06	0.05–0.18	4.3	10	

[a] kcal mol^{-1}.

We next generated double mutant pairs in the nAChR (Table 2) as described previously for the 5-HT_{3A}R. Interestingly, the $\Delta\Delta G^0$ values for each of the double mutants AB, BC, and AC were all near 1.0 kcal mol^{-1}, indicating a similar degree of cooperativity between any two mutations. It is not surprising that mutations to Lys-145 and Asp-200 should be coupled, as previous work has proposed a salt bridge between these residues in the muscle-type nAChR (12). Indeed, analysis via patch clamp electrophysiology of the steady-state dissociation of ACh from the double mutant K145Q/D200N has been previously observed to give a very similar $\Delta\Delta G^0$ value of 1.0 kcal mol^{-1}, and other measures suggest a strong interaction between the two (12). Our observation that both residues also couple to Thr-202 suggests interactions among all three.

The next logical step was to evaluate the functional response to ACh of the triple mutant: $\alpha1$ K145T/D200E/T202K (ABC). The triple mutant receptor was functional, with $EC_{50} = 67 \pm 5.3$ μM ACh, a 4.3-fold increase from wildtype (Table 2). The data from the single, double, and triple mutants enables a triple mutant cycle analysis, which can be represented as a cube (Fig. 3). The difference between each opposite face gives a $\Delta\Delta\Delta G^0$, which quantifies the interaction energy among all three residues as a unit (23). We find in each case that $\Delta\Delta\Delta G^0 = 0.95$ kcal mol^{-1}. That is, any pair of mutations gives $\Delta\Delta G^0 \approx 0.95$ kcal mol^{-1}, but in the background of any single mutation a double mutant cycle of the other two mutations yields $\Delta\Delta G^0 \approx 0$ kcal mol^{-1}. Thus these residues not only interact with one another in the activation mechanism, but operate as a co-dependent unit in the mouse muscle-type nAChR. Each pair of residues is energetically dependent on the third residue of the triad.

To further evaluate the role of this triad, we mutated residues in the 5-HT_{3A}R to their equivalents in $GABA_A$R β-subunits, which form the primary binding face in $GABA_A$Rs. The results are summarized in Table S1. The single mutant at the A site (T152E) showed a 10-fold loss of function, whereas mutation at the C site (K211S) had no functional consequence. The single mutant E209R (B site), however, was nonfunctional up to 800 μM 5-HT. Attempts to transplant the entire $GABA_A$R triad into the 5-HT_{3A}R, T152E/E209R/K211S, yielded no observable response to concentrations of 5-HT as high as 800 μM. Thus, the inhibitory $GABA_A$R appears to behave differently than the excitatory 5-HT_{3A}R and nAChRs. It is also possible, however,

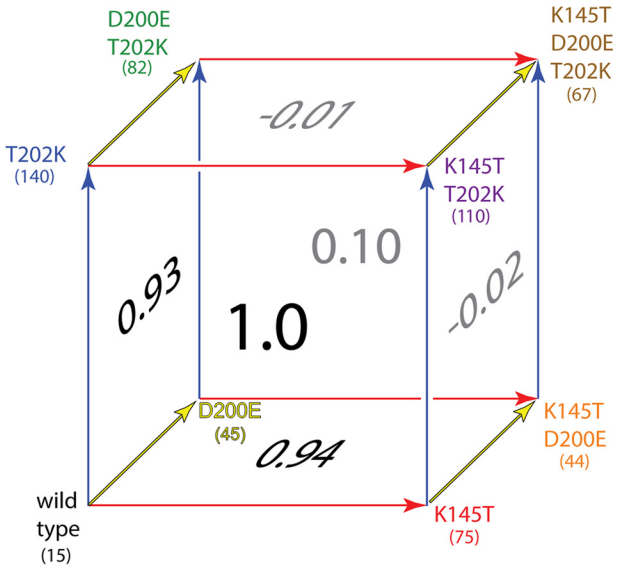

Figure 3. Triple mutant cycle in the muscle-type nAChR. Each face of the cube represents a double mutant cycle. Double mutant cycles from wildtype are meaningfully coupled, however, any pair of mutations is uncoupled in the background of the other mutation of the triad. This analysis yields $\Delta\Delta G$ = 0.95 kcal mol^{-1} for the three mutations. EC_{50} values (μM) are provided in parentheses.

that the receptor mutants, which did not appear to respond to 5-HT, were not expressing or not reaching the cell surface.

Mutating 5-HT$_{3A}$R triad to that of the nAChR increases the binding affinity of nicotine

Having established that 5-HT$_{3A}$Rs incorporating the nAChR-type triad are functional, we next evaluated whether residues in the 5-HT$_{3A}$R triad contribute to the pharmacological properties of nicotine, an agonist of most neuronal nAChRs and a competitive antagonist of 5HT$_{3A}$Rs (1, 24). To accomplish this, we again expressed mutant 5-HT$_{3A}$Rs incorporating the nicotinic-type mutations T152K (A), E209D (B), and K211T (C) as single, double, and triple mutants in *X. laevis* oocytes, and generated Schild plots for inhibition by nicotine for each receptor variant (25, 26). In this procedure, dose-response relationships of each receptor variant were measured in the presence of different concentrations of nicotine. Higher concentrations of nicotine progressively increase the EC_{50} of 5-HT as nicotine displaces 5-HT in the orthosteric binding site (Fig. 4). In a Schild plot, the *x* intercept gives a readout of the equilibrium dissociation constant (K_d) for the antagonist (25, 26).

The Schild plots for each variant are compared with that of the wildtype 5-HT$_{3A}$R in Fig. 5, the parameters of the linear fits are provided in Table S2, and the full pharmacological characterization of the nicotine inhibition experiments is provided in Table S3. The single mutants T152K (A), E209D (B), and K211T (C) increased the K_d of nicotine by 1.5-, 13-, and 2.5-fold, respectively.

Meaningful non-additive effects are observed when the mutations are combined in the double and triple mutants. Despite A and C each producing small increases in the K_d of nicotine, the double mutant AC is 2.2-fold more sensitive to nicotine than wildtype. The double mutant BC is more sensitive to inhibition by nicotine than B on its own, even though C increases the K_d of nicotine on its own. The triple mutant is the most nicotine-sensitive of all the variants, with a K_d 5-fold lower than that of wildtype. Thus these three residues influence the binding of nicotine to the 5-HT$_{3A}$R. In particular, rearranging of Thr-152 (A-site) and Lys-211 (C-site) to their respective positions in nAChRs generates variants that are more sensitive to nicotine inhibition than wildtype. The mutation B, whereas causing a sizable decrease in nicotine affinity on its own, gives a further increase in nicotine sensitivity when combined with the A and C mutations.

This together suggests intimate cooperativity between these three residues in regard to nicotine binding. Mutant cycles of nicotine K_d values (Fig. S5) illustrate meaningful coupling energies between A and C (1.1 kcal mol^{-1}), B and C (0.60 kcal mol^{-1}), and A and B in the background of C (1.2 kcal mol^{-1}).

We attempted to measure inhibition by 5-HT of muscle-type nAChRs containing the 5-HT$_{3A}$R-type triad. However, the results suggested that 5-HT inhibits both wildtype and triple mutant muscle-type nAChRs via a noncompetitive mechanism, consistent with previous work (27). Maximal currents in the presence of 5-HT were decreased, but EC_{50} values of ACh were unchanged (Fig. S6).

The 5-HT$_{3A}$R triad is functionally coupled to nearby residues and the channel gate

Recent structures of Cys-loop receptors show that the triad investigated here is near the agonist-binding site, but none of the residues can directly contact a bound agonist (9–11, 15, 17, 28). The structures do suggest strong interactions between the triad and the canonical loops that position key residues that directly contribute to agonist binding (Fig. S7). It has been previously proposed in the muscle-type nAChR that a strong interaction exists between Lys-145 and Asp-200 (A-site and B-site) in the closed state of the receptor. In the open state this interaction was proposed to be weakened by an interaction between Lys-145 and the OH of Tyr-190, a loop C residue (often referred to as TyrC1) and a completely conserved member of the agonist-binding site aromatic box (12–17). In the $\alpha4\beta2$ nAChR crystal structure (10), Asp-200 interacts with both Lys-145 and Thr-202 (the triad considered here), and the OH of Tyr-190 interacts with both Lys-145 and Asp-200. Recall the crystal structure most likely represents a desensitized state. Very similar interactions are seen in the crystal structure of the nAChR $\alpha2$ ECD (28), crystal structures of acetylcholine-binding protein (17), and in a structure of the $\alpha1$ subunit ECD (15).

In the 5-HT$_{3A}$R the residue that aligns with Tyr-190 is Phe-199, which is unable to make the hydrogen bonding interaction proposed for Tyr-190 of the nAChR. Instead, in the crystal structure the triad of the 5-HT$_{3A}$R makes no apparent contact with loop C, but interacts extensively with Asn-101 and Glu-102 (9), residues that are on the A loop of the agonist-binding site and that have been probed previously. Note that Asn-101 aligns with Tyr-93 (TyrA) of the nAChR, another contributor to the aromatic box (18, 19). In particular, Thr-152 (A site) interacts with the side chain of Glu-102; Glu-209 (B site) interacts with the side chain of Asn-101; and there is also an inter-

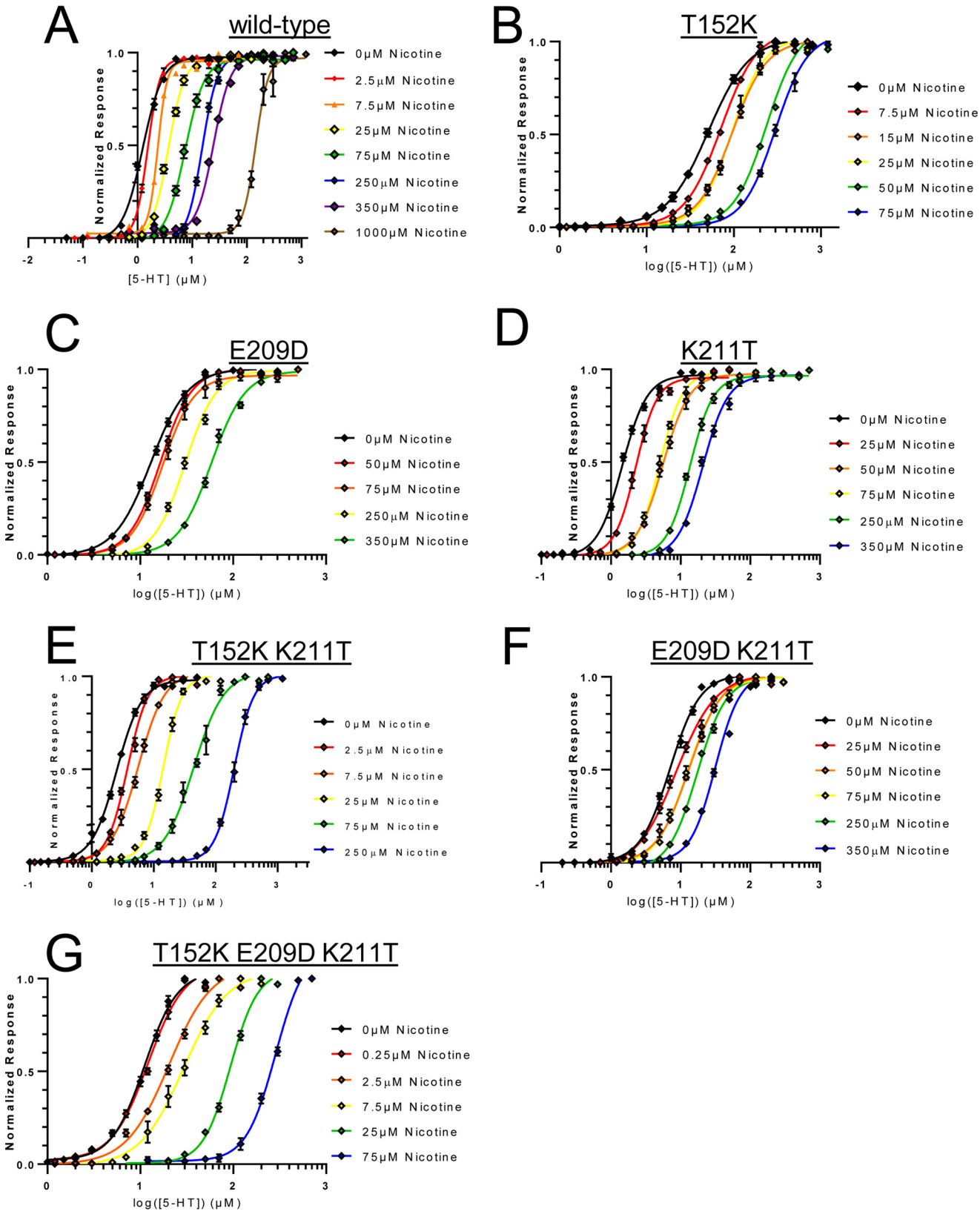

Figure 4. Dose-response curves of 5-HT_{3A}R variants in the presence of varying concentrations of nicotine. As a competitive antagonist, nicotine shifts the dose-response curve of 5-HT_{3A}Rs to higher EC_{50} values. Some variants are more sensitive to competitive inhibition by nicotine than others. *Error bars* represent S.E.

action between the backbone carbonyl of the A site and the backbone NH of Asn-101. The backbone interactions between the A site and the A loop are also present in structures of the nAChR (10) and $GABA_AR$ (11), suggesting an interaction between the triad considered here and the A loop is a universal feature of Cys-loop receptors.

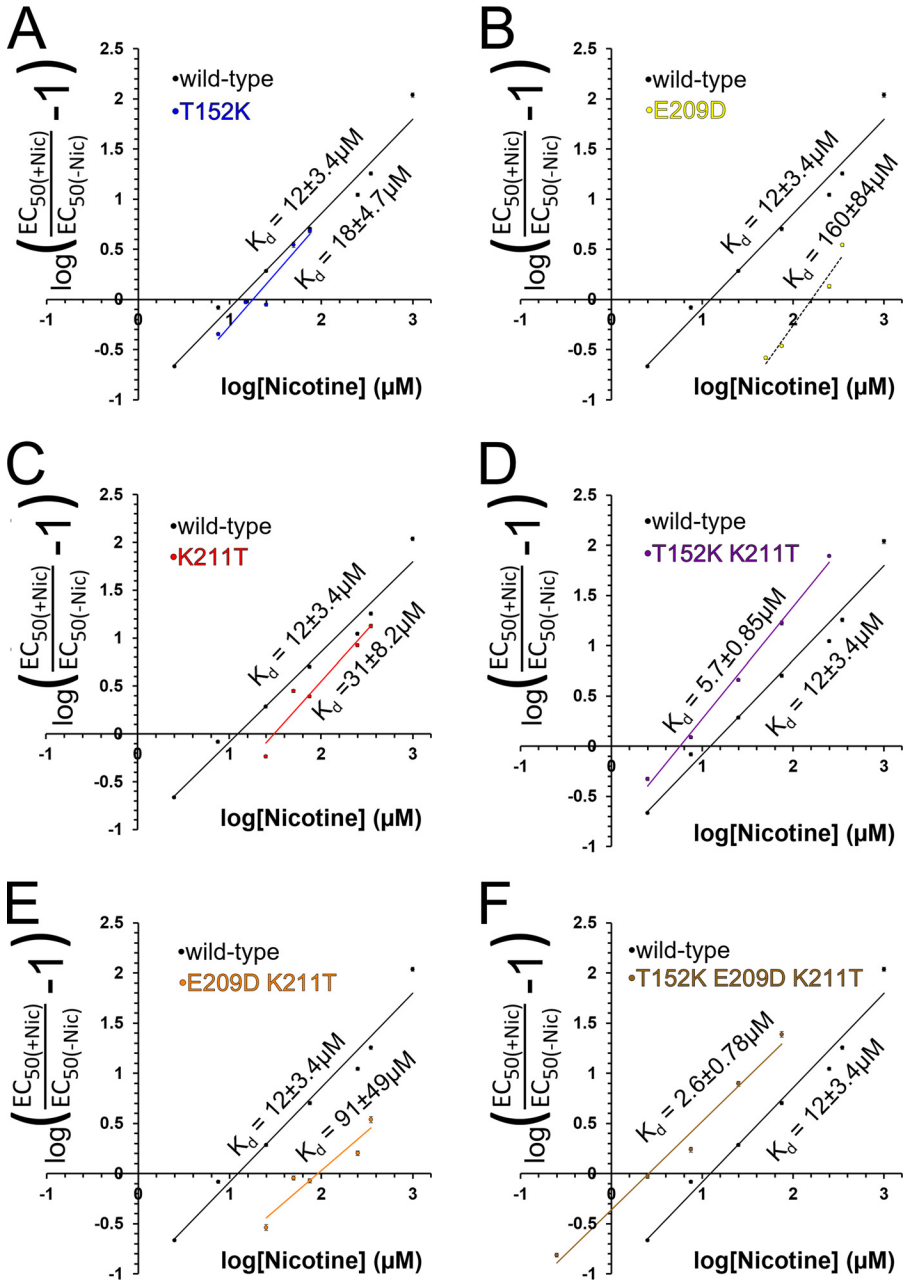

Figure 5. Schild analysis of inhibition of 5-HT$_{3A}$Rs by nicotine. *A–F*, Schild plots comparing inhibition of the wildtype 5-HT$_{3A}$R to the mutants T152K, E209D, K211T, T152K/K211T, E209D/K211T, and T152K/E209D/K211T, respectively. Meaningful changes in nicotine K_d are observed, and the mutations have non-additive effects. Error bars are shown as S.E., and are often smaller than the data points.

We have probed the interactions suggested by the structural work using mutagenesis. For these studies we typically used more conservative mutations than were used in the "triad swapping" experiments (Table 3). For residues Glu-102 and Glu-209, we employ mutations to glutamine and/or aspartate; the E102D mutation was not examined as it has been observed previously that this mutation has little effect on the response of receptors to 5-HT (23). We employ a more drastic mutation at Asn-101, N101K. This was motivated by previous work that demonstrated a high loss of function for the N101K mutation (29). For mutant cycles with Thr-152, we use the conservative T152V mutation.

Table 3 provides the full characterization of the pharmacological response of these receptors to 5-HT. There is extensive cross-talk between the triad and the residues on loop A. All triad residues couple to Asn-101, and Lys-211 couples to Glu-102. Fig. 6 provides a visual depiction of the largest coupling energies observed for pairs of mutations at the sites shown, including those discussed previously and those discussed hereafter. The $\Delta\Delta G^0$ values for different mutant cycles in Fig. 6 are grouped into five categories, each representing an additional 2-fold deviation from additivity.

Previous work in the 5-HT$_{3A}$R on loop A residues Asn-101 and Glu-102 showed that mutations to these residues that introduce a net positive charge (N101K and E102Q) generate very large losses of function (23, 29). This parallels our observation on the T152K mutation, which is the most disruptive of the single mutations in the triad swap. We also observed a large

Table 3

Functional cooperation between triad residues, loop A, Lys-197 (loop C), and the channel gate in mutant 5-HT$_{3A}$Rs

Table is divided into five sections, from top to bottom: 1) single mutants; 2) mutant cycles to N101K and T152V; 3) mutant cycles to the channel gate at T6′; 4) mutant cycles examining role of positive charge; and 5) nonresponsive variants.

Mutation(s)	EC_{50} (μM)	n_H	$\lvert I_{max}\rvert$ (μA)	-Fold	n	$\Delta\Delta G^a$
Wildtype	1.3 ± 0.03	2.4 ± 0.11	1.0–78	1.0	21	
N101K	42 ± 1.1	2.4 ± 0.11	0.05–5.2	34	14	
E102Q	85 ± 3.0	1.6 ± 0.07	0.53–5.5	68	15	
T152V	8.5 ± 0.27	2.2 ± 0.13	0.42–78	6.8	11	
T152K	49 ± 1.0	1.9 ± 0.06	0.14–11	39	15	
K197M	1.5 ± 0.04	2.7 ± 0.19	2.1–20	1.2	10	
E209D	13 ± 0.20	2.3 ± 0.07	0.53–20	10	15	
E209Q	93 ± 4.3	2.4 ± 0.21	2.0–42	75	22	
K211M	2.2 ± 0.05	2.9 ± 0.13	4.9–15	1.8	9	
K211T	1.5 ± 0.04	2.5 ± 0.16	1.9–25	1.2	15	
T6′S	1.3 ± 0.01	4.1 ± 0.17	0.26–17	1.0	22	
N101K/T152V	84 ± 4.0	1.8 ± 0.10	7.2–17	67	16	0.72
N101K/E209D	29 ± 0.17	2.9 ± 0.04	6.7–59	23	17	1.6
T152V/E209D	12 ± 0.21	1.8 ± 0.05	11–23	9.5	13	1.1
T152V/E209Q	96 ± 1.5	2.6 ± 0.09	6.1–87	76	16	1.0
N101K T6′S	11 ± 0.29	1.6 ± 0.07	0.30–23	8.5	11	0.83
E102Q T6′S	5.4 ± 0.28	1.4 ± 0.07	0.10–3.9	4.3	15	1.6
T152V T6′S	1.4 ± 0.10	1.3 ± 0.10	2.3–50	1.1	10	0.98
T152K T6′S	6.6 ± 0.27	2.2 ± 0.16	0.13–2.3	5.3	11	1.2
E209D T6′S	12 ± 0.55	1.9 ± 0.14	0.30–15	9.9	13	0.05
E209Q T6′S	73 ± 8.9	1.1 ± 0.09	0.11–15	58	15	0.17
N101K/K211M	16 ± 0.31	2.0 ± 0.08	0.15–5.5	13	13	0.91
N101K/K211T	15 ± 0.27	3.0 ± 0.16	0.09–4.2	12	15	0.73
E102Q/K211M	8.7 ± 0.15	2.2 ± 0.06	0.28–18	6.9	15	1.7
E102Q/K211T	3.1 ± 0.06	2.6 ± 0.10	6.6–51	2.5	15	2.0
T152K/K211M	31 ± 0.39	2.0 ± 0.04	1.3–18	25	15	0.61
T152K/K211T	2.5 ± 0.05	2.1 ± 0.08	1.3–56	2.0	14	1.8
T152V/K211M	13 ± 0.19	2.3 ± 0.07	2.2–19	10	15	0.05
E209Q/K211M	27 ± 0.28	2.6 ± 0.06	3.2–16	21	14	1.1
E209Q/K211T	15 ± 0.37	2.7 ± 0.15	5.0–16	12	12	1.2
K197M/E209Q	36 ± 0.24	2.8 ± 0.04	4.6–12	29	11	0.65
N101K/K197M	24 ± 1.43	1.9 ± 0.18	0.05–0.74	19	12	0.43
T152K/K197M	32 ± 1.30	1.5 ± 0.08	0.08–1.8	25	10	0.35
N101K/T152K	NR[b]	NR	NR	NR	9	NR
N101K/E209Q	NR	NR	NR	NR	16	NR
E102Q/T152V	NR	NR	NR	NR	10	NR
E102Q/T152K	NR	NR	NR	NR	5	NR
E102Q/E209Q	NR	NR	NR	NR	8	NR
T152K/E209D	NR	NR	NR	NR	15	NR
T152K/K211T/E102Q	NR	NR	NR	NR	9	NR

[a] kcal mol^{-1}.
[b] NR, no response.

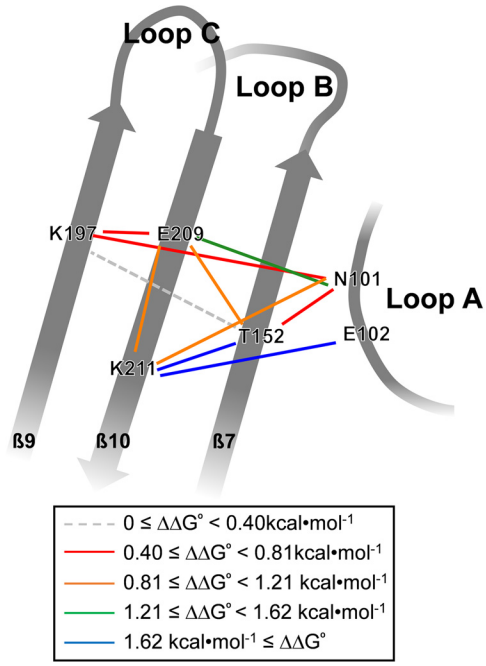

Figure 6. Greatest-magnitude coupling energies observed between pairs of mutations at residues in 5-HT$_{3A}$Rs. Full data can be found in Tables 1 and 3.

loss of function for E209Q, which likewise introduces a net positive charge. In contrast, both K211T and K211M, mutations that remove a positive charge, have minimal impacts on function, but K211T rescued function of receptors with T152K.

In an effort to further probe this ostensible role of positive charge, the single mutants N101K, E102Q, and E209Q, and the double mutants N101K/K211T, E102Q/K211T, and E209Q/K211T were evaluated (Fig. 7; Table 3). We measured $\Delta\Delta G^0$ = 0.73, 2.0, and 1.2 kcal mol^{-1}, respectively, for these three double mutant pairs. Thus all three pairs of mutations are meaningfully coupled, albeit to differing degrees. Recall the large coupling ($\Delta\Delta G^0$ = 1.8 kcal/mol) for T152K/K211T.

We also generated the double mutants around the mutation K211M, the reasoning being that the nonpolar side chain of methionine is sterically similar to the lysine side chain, and does not introduce any other functionalities as in the case of the threonine hydroxyl in K211T. The $\Delta\Delta G^0$ values observed for the double mutants N101K/K211M, E102Q/K211M, T152K/K211M, and E209Q/K211M were 0.91, 1.7, 0.61, and 1.1 kcal mol^{-1}, respectively (Table 3). We also generated the double mutant T152V/K211M, for which the $\Delta\Delta G^0$ value was only 0.05 kcal mol^{-1} (Table 3), demonstrating that a positive charge must be introduced at Thr-152 to couple to Lys-211. Full dose-response curves for mutant cycles examining the role of positive charge among these residues are provided in Fig. S8.

Interestingly, each of the mutations that introduce a net positive charge couple comparably to K211T and K211M, with the exception of T152K. This mutation couples strongly to K211T ($\Delta\Delta G^0$ = 1.8 kcal/mol) but more weakly to K211M ($\Delta\Delta G^0$ = 0.61 kcal/mol). That is to say, the K211T mutation rescues function of T152K more than eight times better than K211M does (Fig. 7*D*). We therefore argue that there is a direct interaction between Thr-152 and Lys-211 in the 5-HT$_{3A}$R, the likes of which cannot be accounted for by merely eliminating the nearby positive charge of the Lys-211 side chain. On the other hand, the deleterious effects of introducing a net positive charge either by introducing N101K, E102Q, or E209Q, are attenuated whenever the basic amine on Lys-211 is removed, regardless of the ability of the residue a position 211 to hydrogen bond.

We also considered another charged residue, Lys-197 that seemed a good candidate for coupling. In the GABA$_A$R, a functionally important salt bridge has been demonstrated between residues aligning to Lys-197 and Thr-152 (30). The 5-HT$_{3A}$R mutation K197M couples weakly to the nearby E209Q ($\Delta\Delta G^0$ = 0.65 kcal mol^{-1}) and N101K ($\Delta\Delta G^0$ = 0.43 kcal/mol), but it does not couple meaningfully T152K ($\Delta\Delta G^0$ = 0.35 kcal mol^{-1}) (Table 3).

Previously, we proposed a strategy for evaluating the role of a particular residue in channel function by evaluating its coupling to a residue in the pore-lining M2 helix that is clearly involved in channel gating (31). In the nAChR, that residue is termed Leu-9′ (the 9th residue from the bottom of the M2 helix). In the

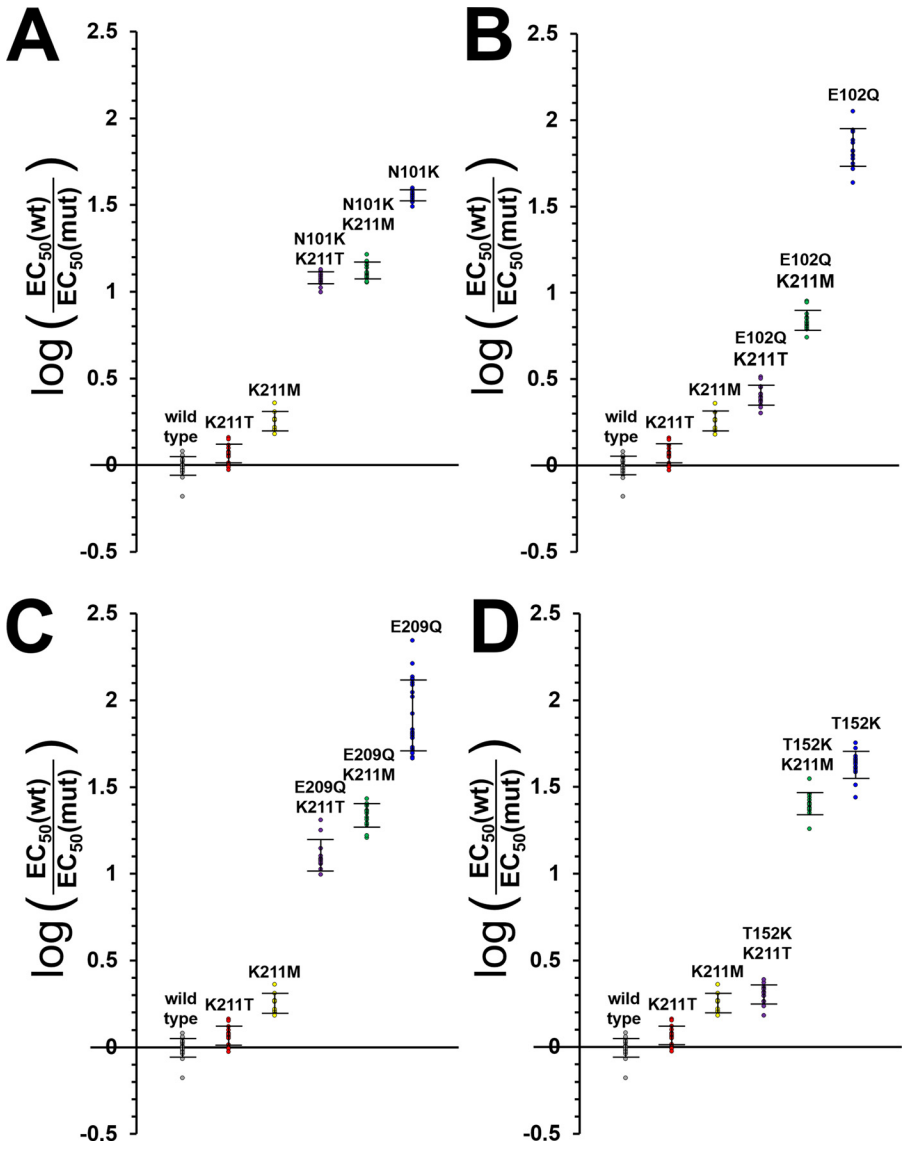

Figure 7. In 5-HT$_{3A}$Rs, mutations that remove the cationic amine on Lys-211 functionally couple to nearby mutations that introduce positive charge. *A*, mutant cycles with N101K. *B*, mutant cycles with E102Q. *C*, mutant cycles with E209Q. *D*, mutant cycles with T152K. Full pharmacological data can be found in Table 3. Dose-response curves provided in Fig. S8. *Error bars* represent S.D.

nAChR we found that D200N couples strongly to L9′A ($\Delta\Delta G$ = 1.3 kcal/mol), establishing a role in gating for Asp-200 (32). However, K145Q and T202Tah (Tah = α-hydroxy threonine, a backbone mutation) do not show strong coupling to L9′A (32).

In the 5-HT$_{3A}$R, the appropriate mutation is T6′S (T257S in our numbering scheme), which has been used extensively to modulate serotonin receptor currents (33). We looked for coupling to T6′S at Asn-101, Glu-102, Thr-152, and Glu-209. The results are summarized in Table 3. We find that N101K, E102Q, T152V, and T152K are all meaningfully coupled to T6′S, suggesting a role in gating for these residues (32). Interestingly, E209D and E209Q do not show meaningful coupling to T6′S. Thus, the nAChR and 5-HT$_{3A}$R show different coupling behaviors to the pore-forming M2 helix. In the nAChR triad, site B couples but sites A and C do not. In the 5-HT$_{3A}$R site A couples and site B does not. We are unable to perform the same analysis for mutations to site C, as none of the mutations we have studied generates an interpretable loss of function relative to wild-type. However, we do note that mutations to site C couple energetically to all of the residues that couple to T6′S.

Attempted expression of the 5-HT$_{3A}$R double mutants E102Q/T152V, E102Q/E209Q, N101K/E209Q, and T152K/N101K yielded no measurable response to high concentrations of 5-HT. This may result either from nonfunctional receptors or a lack of surface expression. Especially for the less-conservative mutations we employ, individual mutations likely affect multiple interactions involved in receptor function, the deleterious effects of which may sometimes add together even if other pairs of mutations at the same sites generate functional receptors.

Discussion

We have identified a triad of residues with one cationic, one anionic, and one hydroxyl-containing side chain that is rearranged between the 5-HT$_{3A}$R, nAChRs, and GABA$_A$Rs, and behaves differently in different receptors. In the muscle-type nAChR, the three triad residues cooperate as a unit, as demon-

strated via triple mutant cycle analysis. This corroborates previous functional and crystallographic work that suggested a salt bridge between two members of the triad is involved in receptor gating (10, 12, 15, 17, 22, 28). We show here that the salt bridge between Lys-145 and Asp-200 depends on Thr-202, which may coordinate this interaction. Mutant cycles of the aligning residues in the 5-HT_{3A}R indicate that Thr-152, Glu-209, and Lys-211 cooperate in the activation mechanism of the 5-HT_{3A}R, but not in a perfectly codependent manner. Interestingly, the triads of the 5-HT_{3A}R and the nAChR can be swapped and still produce functional receptors with minimal loss of function.

The triad of residues in the 5-HT_{3A}R affects the competitive binding of nicotine for the orthosteric site. Each mutation on its own causes a decrease in nicotine binding affinity, although the shift for T152K is very small. Interestingly, however, receptor variants with both the T152K (A) and K211T (C) mutations saw increases in the ability of nicotine to compete with 5-HT relative to wildtype receptors. Moreover, E209D (B), which causes a large loss of nicotine binding affinity on its own, increases the binding affinity for the triple mutant ABC relative to double mutant AC. These three residues thus cooperate in the binding of nicotine, and likely represent a characteristic network of nAChRs. Worth noting is that the only deviations from the cationic/anion/hydroxyl triad of nAChRs are seen in the α9 and α10 nAChRs, which are inhibited rather than activated by nicotine (34). It has been demonstrated elsewhere, however, that mutating the α9 Thr to a Lys does not produce receptors that are activated by nicotine (35), so there is more to it than this one residue.

The triad from the $GABA_A$R does not appear to function in the 5-HT_{3A}R, suggesting this network functions differently in $GABA_A$Rs. Other work has proposed a functionally important salt bridge between residues in the $GABA_A$R aligning to Lys-197 and Thr-152 in the 5-HT_{3A}R (30), however, we do not observe meaningful functional coupling between mutations at these sites in the 5-HT_{3A}R. We also note that the pattern of functionalities in the triad we have studied is not conserved in primary-face α-subunits of inhibitory GlyRs. All this together suggests that the triad of residues behaves similarly in excitatory receptors, but is functionally distinct in inhibitory Cys-loop receptors.

Many amino acid residues that we have considered in this study have been examined previously in regard to ligand binding. Based on radioligand binding studies of the 5-HT_{3A}R antagonist [^{3}H]granisetron, it has been proposed that Thr-152 helps to shape the binding site (36). Mutations to 5-HT_{3A}R residues Glu-209 and Lys-211 have been shown previously to have minimal effect on binding of [^{3}H]granisetron (29, 36). Our results show a minimal effect on nicotine binding for T152K, a modest effect for K211T, and a sizable effect for E209D. Thus these results highlight different binding modes for different competitive antagonists.

We further investigated the involvement of residues in the gating mechanism via mutant cycle analyses to the channel gate mutation T6′S. Loop A residue Asn-101 couples to T6′S, supporting a previous proposition that this residue is involved in receptor gating (29). The mutation E102Q couples to T6′S, in line with a previously published result (23). We observe that the T152K mutation affects ligand binding and also couples to the T6′S; thus we propose that this residue is involved in both binding and gating. Quizzically, mutant cycles between Glu-209 and T6′S do not reveal functional coupling between these residues, despite the previously published observation that Glu-209 does not participate in the binding of [^{3}H]granisetron (36). It is possible that Glu-209 plays different roles in response to 5-HT *versus* granisetron binding, or that Glu-209 participates in a functionally relevant pathway that is not linked to the channel gate at Thr-6′. We have not identified any single mutation to Lys-211 that generates interpretable shifts in 5-HT EC_{50}, so we were unable to perform the same analysis on this residue. However, spatially proximal residues that couple to the channel gate (Asn-101, Glu-102, and Thr-152) also couple to Lys-211.

Mutations that introduce a net positive charge in the region of the 5-HT_{3A}R probed here generally increase the 5-HT EC_{50} by a substantial amount. Most of these large losses of function could be rescued by mutations that remove the side chain amine of Lys-211. An exception is the highly deleterious T152K mutation, which can be nearly fully rescued by the K211T mutation, corresponding to the nAChR swap, but to a much lesser extent by the K211M mutation. This argues for a highly specific interaction between Thr-152 and Lys-211 in the native receptor.

We have demonstrated via mutant cycle analyses that triad residues and loop A residues are functionally coupled in the 5-HT_{3A}R. Structural studies suggest similar interactions between the triad and loop A in nAChR. However, a previously established interaction between triad residues and loop C in nAChRs does not carry over to the 5-HT_{3A}R. These results highlight the fact that there is considerable variation in the degree to which structurally/functionally important features are or are not conserved across members of the Cys-loop family.

Experimental procedures

Molecular biology

The cDNA for the mouse 5-HT_3R A subunit (m5HT_{3A}) was in the pGEMhe vector. The cDNA for the mouse nAChR α1, β1, γ, and δ were in the pAMV vector. The α1 subunit contains a hemagglutinin epitope tag in the M3–M4 loop, which does not alter the EC_{50} of ACh. Site-directed mutagenesis was performed using a QuikChange mutagenesis kit (Stratagene). cDNA was linearized using XhoI (New England Biolabs) for m5-HT_{3A}, XbaI (New England Biolabs) for mα1, or NotI (New England Biolabs) for mβ1, mγ, and mδ subunits. Linearized DNA was purified using a Qiaquick PCR Purification Kit (Qiagen) before performing an *in vitro* runoff transcription using a T7 mMessage mMachine kit (Ambion). The mRNA was purified using an RNEasy Mini Kit (Qiagen) and concentrations were quantified via UV-visible spectroscopy (Nanodrop 2000, ThermoFisher Scientific). cDNA was stored at −20 °C and mRNA was stored at −80 °C.

Protein expression in X. laevis oocytes

Stage V-VI *X. laevis* oocytes were prepared as previously described (37). Oocytes were injected with 50 nl of mRNA in nuclease-free water, and expression levels of different mutants

were optimized by varying mRNA concentrations and incubation times. For experiments involving 5-HT_{3A}R variants, oocytes were injected with 5–50 ng of mRNA once at 24 h before, once at 48 h before, or twice at 24 and 48 h before electrophysiological recording was performed. For experiments involving muscle-type nAChRs, oocytes were injected with a mixture of α1, β1, γ, and δ mRNAs in a 10:5:5:5 ng ratio (per 50 nl) once at 24 h before, once at 48 h before, or twice at 24 and 48 h before electrophysiological recording was performed. Cells were incubated at 18 °C in ND96 (96 mM NaCl, 2 mM KCl, 1 mM $MgCl_2$, 1.8 mM $CaCl_2$, and 5 mM HEPES at pH 7.5) with 0.05 mg/ml of gentamycin (Sigma), 2.5 mM sodium pyruvate (Acros Organics), and 0.67 mM theophylline (Sigma).

Whole cell electrophysiological recording

Electrophysiology and drug perfusion were performed at ambient room temperature (20–25 °C) using the OpusXpress 6000A (Axon Instruments) in two-electrode voltage-clamp mode. Oocytes were impaled with borosilicate glass pipettes filled with 3 M KCl (r = 0.3–3.0 megaohm) and clamped at a holding potential of −60 mV. Data were sampled at 125 Hz. The running buffer was Ca^{2+}-free ND96 (96 mM NaCl, 2 mM KCl, 1 mM $MgCl_2$, and 5 mM HEPES at pH 7.5). Solutions of serotonin hydrochloride (Sigma), acetylcholine chloride (Sigma), and (−)-nicotine tartrate (Sigma) were prepared 0–24 h before recording from stock solutions stored at −80 °C.

For dose-response experiments, 1 ml of each concentration of drug in Ca^{2+}-free ND96 was applied for 15 s followed by a 116-s wash using Ca^{2+}-free ND96 before subsequent doses. For slow-activating variants, 1 ml of drug solution was applied for 15 s and cells were incubated in the drug solution for an additional 15 s before washout. For slow-deactivating variants, washout times were increased to 176 s between doses. The different procedure for slow activating/deactivating variants did not meaningfully change the overall dose-response relationships recorded *versus* the standard 15-s application/116-s wash procedure.

For Schild analysis experiments, cells were continuously perfused with Ca^{2+}-free ND96 containing (−)-nicotine, and 1-ml solutions of 5-HT in Ca^{2+}-free ND96 with the requisite concentration of (−)-nicotine were applied for 15 s/dose, followed by 116-s washes between doses. As in the dose-response experiments, application times and wash times were adjusted for variants displaying slow activation/deactivation.

Data analysis

Raw two-electrode voltage-clamp traces were prepared and analyzed in Clampfit 10.3 (Axon Instruments). Raw data were first filtered using a low pass Gaussian filter at 1 Hz. A 30-s baseline was established prior to each drug application during which cells were continuously perfused with Ca^{2+}-free ND96. The averaged current of the baseline was subtracted from the peak amplitude following each drug application to generate dose-response data.

Dose-response data for individual concentrations were averaged, plotted, and fit to the Hill equation $I/I_{max} = 1/(1 + (EC_{50}/[\text{agonist}]^{nH})$ in Kaleidagraph 3.6 (Synergy), where EC_{50} is the concentration for a half-maximal response, n_H is the Hill coefficient, and I/I_{max} is the normalized response at a given drug concentration. For dose-response experiments, data were normalized to the maximum current observed.

Dose-response curves shown in figures were generated in Prism 7 (GraphPad). The linear fit for the Schild plots were determined in Prism 7, whereas the figure itself was made in Microsoft Excel 2013. The values for the slopes are reported in the text as slope fit ± S.E.

Coupling energies for double-mutant cycles were calculated using the formula $\Delta\Delta G = -R \times T \times \ln((EC_{50wt} \times EC_{50AB})/(EC_{50A} \times EC_{50B}))$, where R is the gas constant, T is temperature, A and B denote individual mutations, and AB denotes double mutant receptors. The value used for T was 293.15 K.

The sequence alignment in Fig. 1*B* was performed in Clustal Omega using sequences from Uniprot corresponding to the following accession numbers: P46098 (human 5-HT_{3A}), P02708 (human α1 nAChR), Q15822 (human α2 nAChR), P32297 (human α3 nAChR), P43681 (human α4 nAChR), P30532 (human α5 nAChR), Q15825 (human α6 nAChR), P36544, (human α7 nAChR), Q9UGM1 (human α9 nAChR), Q9GZZ6 (human α10 nAChR), P18505 (human β1 $GABA_A$), P47870 (human β2 $GABA_A$), and P28472 (human β3 $GABA_A$).

Author contributions—R. M. and D. A. D. designed the study and prepared the manuscript. All laboratory work was conducted by R. M. Both R. M. and D. A. D. analyzed the results and approved the final version of the manuscript.

Acknowledgments—We thank Prof. Henry A. Lester and Prof. Sarah Lummis for helpful discussions.

References

1. Albuquerque, E. X., Pereira, E. F., Alkondon, M., and Rogers, S. W. (2009) Mammalian nicotinic acetylcholine receptors: from structure to function. *Physiol. Rev.* **89,** 73–120 CrossRef Medline
2. Sigel, E., and Steinmann, M. E. (2012) Structure, function, and modulation of GABAA receptors. *J. Biol. Chem.* **287,** 40224–40231 CrossRef Medline
3. Betz, H., and Laube, B. (2006) Glycine receptors: recent insights into their structural organization and functional diversity. *J. Neurochem.* **97,** 1600–1610 CrossRef Medline
4. Lummis, S. C. R. (2012) 5-HT3 receptors. *J. Biol. Chem.* **287,** 40239–40245 CrossRef Medline
5. Thompson, A. J., and Lummis, S. C. (2007) The 5-HT3 receptor as a therapeutic target. *Expert Opin. Ther. Targets.* **11,** 527–540 CrossRef Medline
6. Miller, P. S., and Smart, T. G. (2010) Binding, activation and modulation of Cys-loop receptors. *Trends Pharmacol. Sci.* **31,** 161–174 CrossRef Medline
7. Lynagh, T., and Pless, S. A. (2014) Principles of agonist recognition in Cys-loop receptors. *Front. Physiol.* CrossRef
8. Thompson, A. J., Lester, H. A., and Lummis, S. C. (2010) The structural basis of function in Cys-loop receptors. *Q. Rev. Biophys.* **43,** 449–499 CrossRef Medline
9. Hassaine, G., Deluz, C., Grasso, L., Wyss, R., Tol, M. B., Hovius, R., Graff, A., Stahlberg, H., Tomizaki, T., Desmyter, A., Moreau, C., Li, X.-D., Poitevin, F., Vogel, H., and Nury, H. (2014) X-ray structure of the mouse serotonin 5-HT3 receptor. *Nature* **512,** 276–281 CrossRef Medline
10. Morales-Perez, C. L., Noviello, C. M., and Hibbs, R. E. (2016) X-ray structure of the human $\alpha4\beta2$ nicotinic receptor. *Nature* **538,** 411–415 CrossRef Medline
11. Miller, P. S., and Aricescu, A. R. (2014) Crystal structure of a human GABAA receptor. *Nature* **512,** 270–275 CrossRef Medline

12. Mukhtasimova, N., Free, C., and Sine, S. M. (2005) Initial coupling of binding to gating mediated by conserved residues in the muscle nicotinic receptor. *J. Gen. Physiol.* **126,** 23–39 CrossRef Medline
13. Nasiripourdori, A., Ranjbar, B., and Naderi-Manesh, H. (2009) Binding of long-chain α-neurotoxin would stabilize the resting state of nAChR: a comparative study with α-conotoxin. *Theor. Biol. Med. Model.* **6,** 3 CrossRef Medline
14. Horenstein, N. A., McCormack, T. J., Stokes, C., Ren, K., and Papke, R. L. (2007) Reversal of agonist selectivity by mutations of conserved amino acids in the binding site of nicotinic acetylcholine receptors. *J. Biol. Chem.* **282,** 5899–5909 CrossRef Medline
15. Dellisanti, C. D., Yao, Y., Stroud, J. C., Wang, Z.-Z., and Chen, L. (2007) Crystal structure of the extracellular domain of nAChR α1 bound to α-bungarotoxin at 1.94-Å resolution. *Nat. Neurosci.* **10,** 953–962 CrossRef Medline
16. Mallipeddi, P. L., Pedersen, S. E., and Briggs, J. M. (2013) Interactions of acetylcholine binding site residues contributing to nicotinic acetylcholine receptor gating: role of residues Y93, Y190, K145 and D200. *J. Mol. Graph. Model.* **44,** 145–154 CrossRef Medline
17. Celie, P. H., van Rossum-Fikkert, S. E., van Dijk, W. J., Brejc, K., Smit, A. B., and Sixma, T. K. (2004) Nicotine and carbamylcholine binding to nicotinic acetylcholine receptors as studied in AChBP crystal structures. *Neuron* **41,** 907–914 CrossRef Medline
18. Taly, A., Corringer, P.-J., Guedin, D., Lestage, P., and Changeux, J.-P. (2009) Nicotinic receptors: allosteric transitions and therapeutic targets in the nervous system. *Nat. Rev. Drug Discov.* **8,** 733–750 CrossRef Medline
19. Dougherty, D. A. (2013) The cation–π interaction. *Acc. Chem. Res.* **46,** 885–893 CrossRef Medline
20. Horovitz, A. (1996) Double-mutant cycles: a powerful tool for analyzing protein structure and function. *Fold. Des.* **1,** R121–R126 CrossRef Medline
21. Xiu, X., Puskar, N. L., Shanata, J. A., Lester, H. A., and Dougherty, D. A. (2009) Nicotine binding to brain receptors requires a strong cation–π interaction. *Nature* **458,** 534–537 CrossRef Medline
22. Unwin, N. (2005) Refined structure of the nicotinic acetylcholine receptor at 4-Å resolution. *J. Mol. Biol.* **346,** 967–989 CrossRef Medline
23. Miles, T. F., Bower, K. S., Lester, H. A., and Dougherty, D. A. (2012) A coupled array of noncovalent interactions impacts the function of the 5-HT3A serotonin receptor in an agonist-specific way. *ACS Chem. Neurosci.* **3,** 753–760 CrossRef Medline
24. Gurley, D. A., and Lanthorn, T. H. (1998) Nicotinic agonists competitively antagonize serotonin at mouse 5-HT3 receptors expressed in *Xenopus* oocytes. *Neurosci. Lett.* **247,** 107–110 CrossRef Medline
25. Colquhoun, D. (2007) Why the Schild method is better than Schild realised. *Trends Pharmacol. Sci.* **28,** 608–614 CrossRef Medline
26. Wyllie, D. J., and Chen, P. E. (2007) Taking the time to study competitive antagonism. *Br. J. Pharmacol.* **150,** 541–551 Medline
27. Cross, K. M., Foreman, R. C., and Chad, J. E. (1995) Enhancement by 5-hydroxytryptamine and analogues of desensitization of neuronal and muscle nicotinic receptors expressed in *Xenopus* oocytes. *Br. J. Pharmacol.* **114,** 1636–1640 CrossRef Medline
28. Kouvatsos, N., Giastas, P., Chroni-Tzartou, D., Poulopoulou, C., and Tzartos, S. J. (2016) Crystal structure of a human neuronal nAChR extracellular domain in pentameric assembly: ligand-bound α2 homopentamer. *Proc. Natl. Acad. Sci.* **113,** 9635–9640 CrossRef Medline
29. Price, K. L., Bower, K. S., Thompson, A. J., Lester, H. A., Dougherty, D. A., and Lummis, S. C. (2008) A hydrogen bond in loop A is critical for the binding and function of the 5-HT3 receptor. *Biochemistry* **47,** 6370–6377 CrossRef Medline
30. Venkatachalan, S. P., and Czajkowski, C. (2008) A conserved salt bridge critical for GABAA receptor function and loop C dynamics. *Proc. Natl. Acad. Sci. U.S.A.* **105,** 13604–13609 CrossRef Medline
31. Shanata, J. A. P., Frazier, S. J., Lester, H. A., and Dougherty, D. A. (2012) Using mutant cycle analysis to elucidate long-range functional coupling in allosteric receptors. *Methods Mol. Biol.* **796,** 97–113 CrossRef
32. Gleitsman, K. R., Shanata, J. A., Frazier, S. J., Lester, H. A., and Dougherty, D. A. (2009) Long-range coupling in an allosteric receptor revealed by mutant cycle analysis. *Biophys. J.* **96,** 3168–3178 CrossRef Medline
33. Thompson, A. J., and Lummis, S. C. (2013) A single channel mutation alters agonist efficacy at 5-HT3A and 5-HT3AB receptors. *Br. J. Pharmacol.* **170,** 391–402 CrossRef Medline
34. Giastas, P., Zouridakis, M., and Tzartos, S. J. (2017) Understanding structure-function relationships of the human neuronal acetylcholine receptor: insights from the first crystal structures of neuronal subunits. *Br. J. Pharmacol.* CrossRef
35. Zouridakis, M., Giastas, P., Zarkadas, E., Chroni-Tzartou, D., Bregestovski, P., and Tzartos, S. J. (2014) Crystal structures of free and antagonist-bound states of human α9 nicotinic receptor extracellular domain. *Nat. Struct. Mol. Biol.* **21,** 976–980 CrossRef Medline
36. Thompson, A. J., Price, K. L., Reeves, D. C., Chan, S. L., Chau, P.-L., and Lummis, S. C. (2005) Locating an antagonist in the 5-HT3 receptor binding site using modeling and radioligand binding. *J. Biol. Chem.* **280,** 20476–20482 CrossRef Medline
37. Dougherty, D. A., and Van Arnam, E. B. (2014) *In vivo* incorporation of unnatural amino acids using the chemical aminoacylation strategy: a broadly applicable mechanistic tool. *Chembiochem* **15,** 1710–1720 CrossRef Medline